IEEE Access
Multidisciplinary | Rapid Review | Open Access Journal

Received 4 June 2022, accepted 3 July 2022, date of publication 15 July 2022, date of current version 1 August 2022.

*Digital Object Identifier 10.1109/ACCESS.2022.3191424*

RESEARCH ARTICLE

# Experimental Study on the Break-In Process of a Differential Redundant Actuation System Based on the Rudder Loop Load Simulation Platform

**PEIJUAN CUI[1,2,3], QIANFAN ZHANG[1], (Member, IEEE), ZHANLIN HOU[2,3], YUPING HUANG[2,3], LUMAN HE[2,3], AND ZAIPING ZHENG[1,2,3]**

[1]School of Electrical Engineering and Automation, Harbin Institute of Technology, Harbin 150001, China
[2]Beijing Institute of Precision Mechatronics and Controls, Beijing 100076, China
[3]Laboratory of Aerospace Servo Actuation and Transmission, Beijing 100076, China

Corresponding author: Qianfan Zhang (zhang_qianfan@hit.edu.cn)

**ABSTRACT** The break-in operation of the brake unit of a differential redundant actuation system is of considerable importance to improve its reliability and safety. However, the operation will generate a large impact on the driven load, which may cause damage to the load, and hence, it needs to be analyzed in detail. In this study, we first analyzed in detail the different working modes of a differential redundant actuation system and their dynamic characteristics during the break-in process. Subsequently, a dedicated offline test platform for the load simulation of the actuation system was designed to simulate rudders, i.e., the main type of load for such an actuation system. The test platform was used to perform experimental testing on the impact characteristics of the break-in process on the load under different working modes of the actuation system, and the relevant test data were obtained and evaluated accordingly. The experimental results show that, when the differential redundant actuation system is in a multiple-degrees-of-freedom state with a single input and multiple outputs, the break-in process of the brake unit has the smallest impact on the load; furthermore, when the backup channel of the differential redundant actuation system is in a locked state, the break-in process of the brake unit has the largest impact on the load.

**INDEX TERMS** Actuation system, break-in process, experimental studies, load simulation platform.

## I. INTRODUCTION

A differential redundant actuation system is a redundant actuation system that uses a mechanical electromagnetic brake as the core braking unit for fault isolation and reconfiguration in a two-degrees-of-freedom system. It has a clear fault isolation interface, which can fundamentally solve the force fighting of multiple motors in redundant actuation systems [1]–[3]. However, due to the influence of the environment and load during service, the iron-based friction pair surface of the braking unit of a differential redundancy actuation system will undergo degradation phenomena like oxidation, resulting in the problem that the braking torque will gradually decay with the increase of service time, which reduces the reliability of the entire system [4]. Studies have shown that the break-in operation of the brake unit can effectively improve the work surface status of the friction pair and restore the braking performance, thus fully improving the reliability and safety of the operating system [5], [6].

The friction process of the brake unit of a differential redundant actuation system involves surface friction of the low pair. In the existing literature on the break-in process, Sun [7] regarded the break-in wear process as a black box from the perspective of system science, and established a prediction model for the characteristic parameters of the break-in attractor without relying on the theory of wear. For the friction pair surface, the initial surface roughness of the softer material should be processed to a small amplitude, but it takes a wide range of values. Zhang [8] created an analytical model of the break-in wear of the sliding friction

The associate editor coordinating the review of this manuscript and approving it for publication was Chih-Yu Hsu.

pair based on the theory of contact mechanics, and utilized the break-in as a black-box process for machine learning to avoid the bias caused by the simplification of the break-in process. The author established the correlation between the input variables (running conditions and surface topography) and the output variables (surface topography or break-in wear) of the break-in process to predict the characteristics of the break-in wear based on the surface topography of the friction pair. Zhang *et al.* [9] investigated the tribological design of the break-in process, and analyzed the influence of factors, such as the speed of the internal combustion engine, load, the initial surface roughness of the cylinder liner and piston ring, and lubricant viscosity, on the break-in process of the internal combustion engine via the mathematical modeling of the break-in process.

The brake units of differential redundant actuation systems often have to be broken in while in service; hence, the shock loads generated by the brake units during break-in are transmitted to loads, such as the rudder, through the transmission chain of the actuation system, thus potentially damaging the connected loads [10]–[12]. On the other hand, the dual mechanical input channels of the differential redundant actuation system allow a wide range of working modes to be selected, and the impact of the break-in operation on the load varies among different working modes [14], [15]. The above problems are difficult to be analyzed through an online line inspection of the break-in process of the actuation system. Therefore, an appropriate offline simulation test platform needs to be designed for the break-in process of the actuation system, and the impact of the break-in process on the transmission chain and the load should be studied in-depth under different working modes to provide a reasonable evaluation.

To address the above issues, we first analyzed in detail the different working modes of the differential redundant actuation system and their dynamics during the break-in process. Subsequently, a dedicated offline test platform for the load simulation of the actuation system was designed to simulate rudders, i.e., the main type of load for such an actuation system. The elastic load, inertia load and friction load of the air rudder were simulated. In order to ensure the stability of the loading process, a full stroke spring preloading loading method was proposed. The test platform was used to conduct experimental testing on the impact characteristics of the actuation system on the load during the break-in process under different working modes, and the relevant test data were obtained and evaluated accordingly. In this study, we used experimental testing to challenge the conventional thinking of the break-in of actuation systems in the working channel, and discussed and evaluated various feasible break-in working modes of the actuation system by changing the constraint modes and transmission channels of the redundant actuation system in order to explore and propose a break-in working mode that produces the lowest peak impact force on the rudder surface.

## II. ANALYSIS OF THE DIFFERENTIAL REDUNDANT ACTUATION SYSTEM AND THE WORKING MODES DURING BREAK-IN

In this section, we described the working principle of the differential redundant actuation system, and conducted a theoretical analysis on the dynamic characteristics of the brake unit during the break-in process.

### A. WORKING PRINCIPLE OF DIFFERENTIAL REDUNDANT ACTUATION SYSTEM AND ITS BREAK-IN AND LOCK WORKING MODE

A differential redundant actuation system mainly consists of a control and drive apparatus, a servo motor (i.e., the AC permanent magnet synchronous servo motor), an electromagnetic brake, a dual-input planetary gear differential, and a ball screw pair, as shown in Fig. 1.

This system has two relatively independent input channels A and B, each with its own servo motor and electromagnetic brake, which are arranged coaxially and serially, and their function is to brake or start the one-way input power, to switch the working modes, and to achieve system fault isolation and reconfiguration. The servo motor of the two channels is connected to the satellite differential, and the corresponding torque of the screw pairs is output by the differential motion to enable the motion of the rudder surface and other loads.

When the control center sends a position command to the actuation system, the position command is compared with the feedback signal of the actuator displacement sensor to obtain the position error, and the actuation system driver controls the dual-redundant motor to convert electrical energy to mechanical energy and outputs the controllable speed and electromagnetic torque. The output power of the motor is then fed into the mechanical drive, which decelerates and rotates into a straight line and outputs the controllable force and speed, which in turn drives the load.

Based on the transmission characteristics of the differential redundant actuation system, the system has various working modes, and the break-in working mode of the brake unit may not be limited to the normal working mode of the actuation system itself and its connection mode. When break-in applies to Channel A, under the premise of satisfying more than one degree of freedom on the force transmission path, both Channel B and the rudder surface have two working status options, i.e., free and fixed, which can form the following three possible constraints, as shown in Table 1. As the impact on the rudder surface and other loads during the break-in process is different depending on the path, all the working modes should be explored and the optimal break-in working mode should be proposed.

### B. ANALYSIS OF DYNAMIC CHARACTERISTICS OF THE BREAK-IN PROCESS OF DIFFERENTIAL REDUNDANT ACTUATION SYSTEM

The dynamics of the transmission paths under the three abovementioned working modes are investigated considering the transmission characteristics of the dual-input differential.

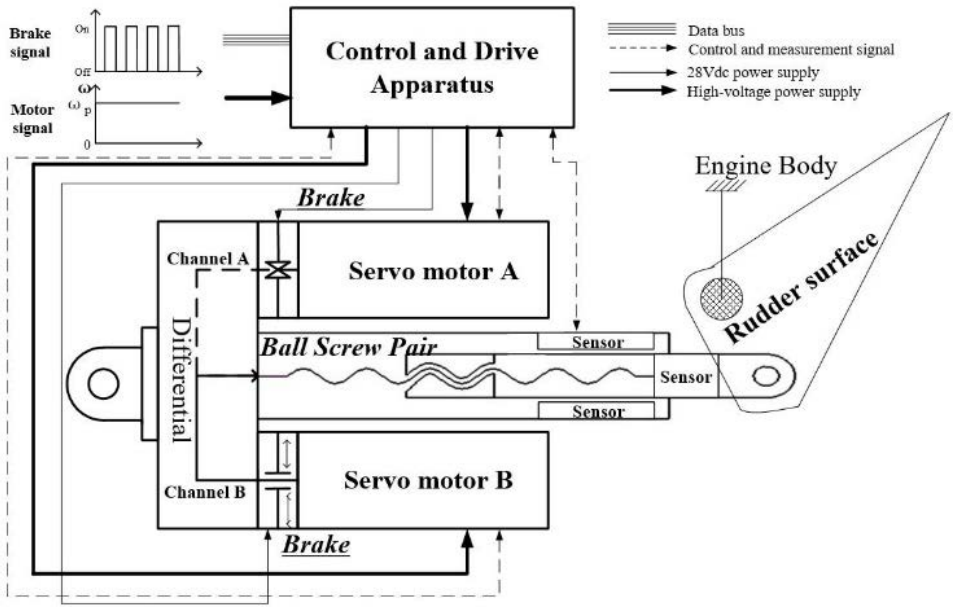


**FIGURE 1.** Schematic of the differential redundant actuation system.

**TABLE 1.** Break-in combinations of the differential redundant actuation system.

| Working mode | Rudder surface status | Channel B status | Loop degrees of freedom |
|---|---|---|---|
| Mode 1 | Fixed | Free | 1 |
| Mode 2 | Free | Fixed | 1 |
| Mode 3 | Free | Free | 2 |

Under Mode 1, the system is a single-input and single-output system. At this time, Channel A is in the break-in state, the simulated load in the actuation system is in the fixed state, and Channel B is in the free state. Meanwhile, the input torque of Motor A is transmitted to the planetary gear differential through the drive shaft by the brake, and as the ball screw pair is fixed with the load end, Gear 1 transmits the torque to Gear 6 through Gear 2 and Gear 5 to drive the rotation of Motor B. The system diagram and main dynamic parameters are shown in Fig. 2.

Under this working mode, the working channel, Channel A, only needs to overcome the sum of the frictional torque $T_{fAB}$ between Channels A and B and the no-load torque $T_{mB0}$ ripple of the Channel B motor. As the controlled motor is controlled at a uniform speed in an unlocked state, the load on the controlled input is balanced against the system resistance, and the torque $T_{1mA}$ on the controlled input A under Mode 1 is shown in (1).

$$T_{1mA} = T_{fAB} + T_{mB0} \tag{1}$$

Under Mode 2, the system is a single-input and single-output system. At this time, Channel A is in the broken-in and locked state, the rudder surface and other loads in the

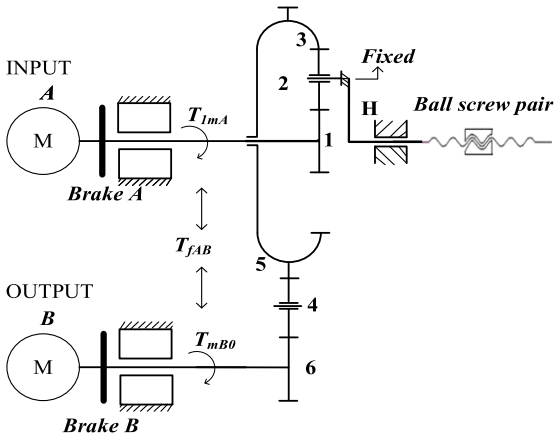


**FIGURE 2.** System motion relations and main dynamic parameters under break-in mode 1.

actuation system are in the free state, and Channel B is in the fixed state. When Gear 6 and Gear 4 are then fixed, the input torque of the motor is transmitted to the planetary gear differential by the brake, and Gear 1 drives the torque through Gear 2 to drive the motion of the ball screw pair to drive the load. The system diagram and main dynamic parameters are shown in Fig. 3.

In this case, the working channel, Channel A, only needs to overcome the frictional torque between channel A and the rudder surface load. In the motion loop, the frictional resistance torque $T_{fAL}$ between Channel A and the load includes the frictional resistance torque $T_{fAH}$ from the input of Differential A to the output of the planetary carrier, the frictional resistance torque $T_{fac}$ of the actuator assembly (including the screw, support bearing, and guide mechanism),

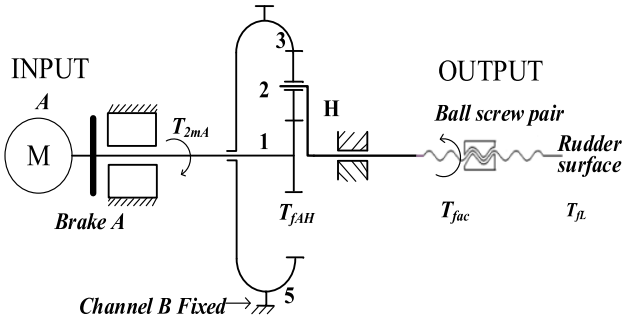


**FIGURE 3.** System motion relations and main dynamic parameters under break-in mode 2.

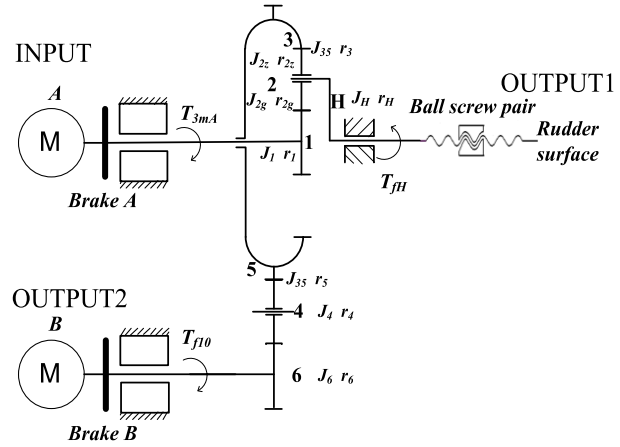


**FIGURE 4.** System motion relations and main dynamic parameters under break-in mode 3.

and the frictional resistance torque $T_{fL}$ of the load. The torque $T_{2mA}$ of the controlled input A is expressed in the following equation:

$$T_{2mA} = T_{fAL} \tag{2}$$

Under Mode 3, the system is a single-input and double-output system, when Channel A is in the broken-in and locked state, and the rudder surface and other loads in the actuation system as well as Channel B are in the free state. Meanwhile, the input torque of Channel A is divided into two parts according to the kinematics of the differential planetary gear, part of which involves the rotation of Gear 2, driving Gear 3 to Gear 6, which in turn drives the Channel B motor; the other part involves the revolution of Gear 2, driving the motion of the ball screw pair, to drive the rudder surface and other loads. The system diagram and main dynamic parameters are shown in Fig. 4.

The dynamical behavior of the system under Mode 3 is relatively complex and is directly related to the frictional resistance situation in the motion transmission channels with large uncertainties.

Based on rigid body dynamics, the relationship between torque and acceleration is derived in the dual-redundancy differential actuation system, the results are shown as follows.

$$\begin{cases} \varepsilon_1 = \dfrac{A_{22}T_0 - \left(A_{22}\left(1+\frac{r_3}{r_1}\right) - A_{12}\frac{r_3}{r_1}\right)T_1 - A_{12}\frac{r_4}{r_6}T_6}{A_{11}A_{22} - A_{21}A_{12}} \\ \varepsilon_6 = \dfrac{A_{21}T_0 - \left(A_{21}\left(1+\frac{r_3}{r_1}\right) - A_{11}\frac{r_3}{r_1}\right)T_1 - A_{11}\frac{r_4}{r_6}T_6}{A_{12}A_{21} - A_{11}A_{22}} \end{cases} \tag{3}$$

where

$$A_{11} = \left(4J_{2g} + J_H + \frac{4J_{2z}r_3}{r_2}\frac{Z_3}{Z_2}\right)\frac{Z_1}{Z_1+Z_3} + J_1 + \frac{J_1 r_3}{r_1} \tag{4}$$

$$A_{12} = \left(4J_{2g} + J_H - \frac{4J_{2z}r_3}{r_2}\frac{Z_1}{Z_2}\right)\frac{Z_3Z_6}{(Z_1+Z_3)Z_4} \tag{5}$$

$$A_{21} = \frac{J_1 r_3}{r_1} + \frac{4J_{2z}Z_1Z_3r_3}{Z_2(Z_1+Z_3)r_2} \tag{6}$$

$$A_{22} = -\frac{4J_{2z}Z_1Z_3Z_6r_3}{Z_2Z_4(Z_1+Z_3)r_2} - \frac{J_{34}Z_6}{Z_4} - \frac{J_5Z_6r_4}{Z_5r_5} - \frac{J_6r_4}{r_6} \tag{7}$$

The motion relation in this process is:

$$i_{13}^H = \frac{\omega_1 - \omega_H}{\omega_3 - \omega_H} = \frac{\varepsilon_1 - \varepsilon_H}{\varepsilon_3 - \varepsilon_H} = -\frac{Z_3}{Z_1} \tag{8}$$

$$n_4 = -\frac{Z_6}{Z_4}\frac{Z_8}{Z_7}n_8 \tag{9}$$

For the planetary gear, because the inner- outer ring gears are controlled by the closed-loop speed of the motor, the tangential speed at the meshing point between the planetary gear and the inner gear is a constant, that is, $n_4 r_3$ is a constant.

To achieve this uniform rectilinear motion, the force balance relationship of the system needs to be discussed. Under the no-load operation condition, the output torque $T_{3mA}$ of Channel A needs to form a balance relationship with the frictional resistance torques $T_{f1o}$ and $T_{fH}$ of the two output channels, that is, the motive force $F_3$ of the system is balanced against the frictional resistances of the two output channels. Only if the balance condition is satisfied can uniform rectilinear motion be achieved.

The planetary gear is the key to the balance analysis, and its force balance equations can be expressed as

$$\begin{cases} -F_3r_2 + f_{1o}r_2 - J_{2z}\varepsilon_{2z} = 0 \\ f_Hr_H - F_3r_3 - f_{1o}r_1 - J_{2g}\varepsilon_{2g} = 0 \\ f_H - F_3 - f_{1o} - m_2\varepsilon_{2g}r_H = 0 \end{cases} \tag{10}$$

where r is the radius of rotation of each gear, $\varepsilon$ is the angular acceleration of each gear. $f_{1o}$ and $f_H$ are the frictional resistances of the two output channels; they are unknown inherent nonlinear parameters associated with the frictional characteristics of the system. The known transmission parameters of the system are substituted, and the relationships among $F_3$, $\varepsilon_{2z}$, and $\varepsilon_{2g}$ are determined. Through the discussion, the following patterns are observed:

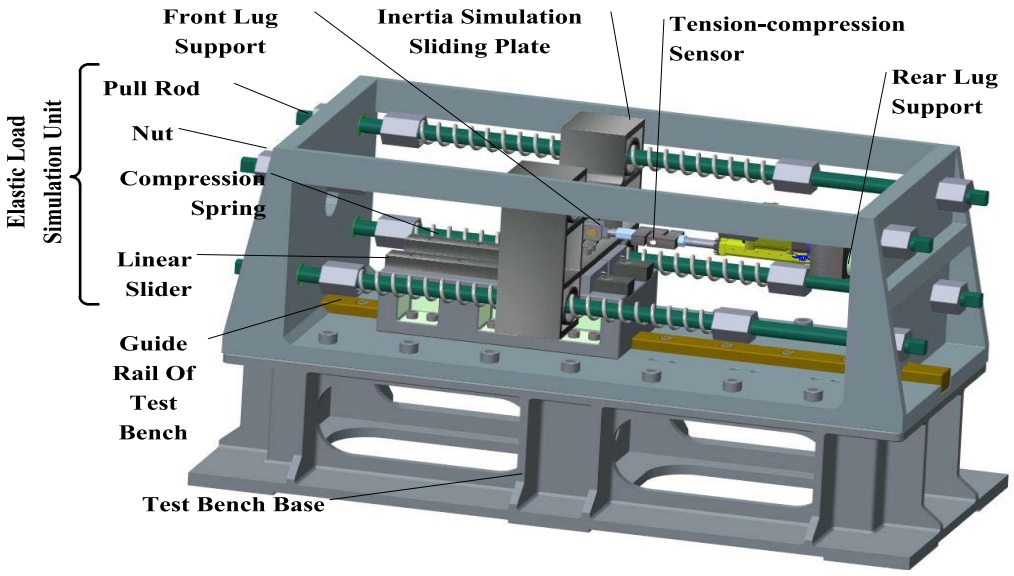


**FIGURE 5.** Schematic of the load simulation platform of the actuation system.

(1) When $f_{1o} = 59/85\, f_H$, the planetary gear rotates and revolves at a uniform velocity.

(2) When $f_{1o} > 59/85\, f_H$, $F_3 \in [f_H, f_1]$, the planetary gear rotates with negatively accelerated motion.

(3) When $f_{1o} < 59/85\, f_H$, $F_3 \in [f_1, f_H]$, the planetary gear rotates with accelerated motion.

Therefore, under Mode 3, the kinematics of the system are related to the magnitude of the frictional resistances $f_{1o}$ and $f_H$ of the two output channels.

## III. LOAD SIMULATION PLATFORM DESIGN OF ACTUATION SYSTEM

The keys to the platform design include the effective simulation of the load, the realization of the driving of the actuator under various working modes through a reasonable design of the control and test system, and the detection of the load impact signals.

### A. STRUCTURAL DESIGN OF THE SIMULATION PLATFORM

The load simulation platform of the actuation system mainly contains an elastic load simulation unit, an inertial load simulation unit, and a friction load simulation unit, as shown in Fig. 5.

In this system, the slewing torque of loads, such as the rudder surface, is high [15]. On the other hand, the linear load transformed to the electromechanical actuator (EMA) via the loop rocker-arm linkage mechanism is relatively low, and the load of the entire load simulation system is in the axial direction. Therefore, the torque that drives the load is transformed into a linear pull pressure load acting in the direction of the linear motion of the EMA to meet the needs of the compact design of a load simulation system for a multi-integrated simulation system (including force, thermal, pneumatic, and other environmental simulations).

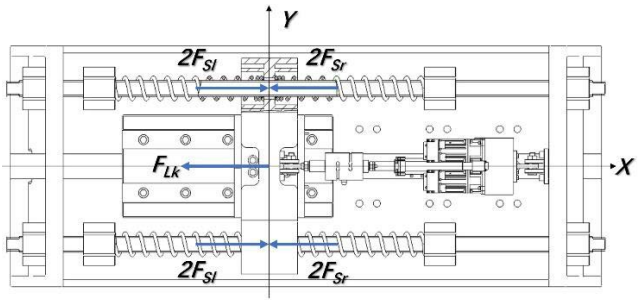


**FIGURE 6.** Force analysis of the elastic load simulation unit.

The elastic load simulation unit mainly simulates the pneumatic elastic load of the rudder load, which consists of a cylindrical compression spring, a pull rod, a nut, a linear slider, and other elements. The elastic load is simulated by adjusting the compression of eight cylindrical springs. To ensure that the eight compression springs are loaded simultaneously, the pre-load is greater than the maximum stroke of the EMA during the test, and the size of the elastic load is directly related to the position. The force analysis of this unit is shown in Fig. 6.

Considering the design of spring preload in this experimental system, the loading force of a single spring can be expressed as

$$F_{Sr} = k_{SS}\,(L_0 + x) \tag{11}$$

$$F_{Sl} = k_{SS}\,(L_0 - x) \tag{12}$$

Based on the force balance, the total elastic loading force can be expressed as

$$F_{Lk} = 4F_{Sl} - 4F_{Sr} = -8k_{SS}x \tag{13}$$

Consequently, the load on this load simulation platform linearly transforms with the operating position of the actuator,

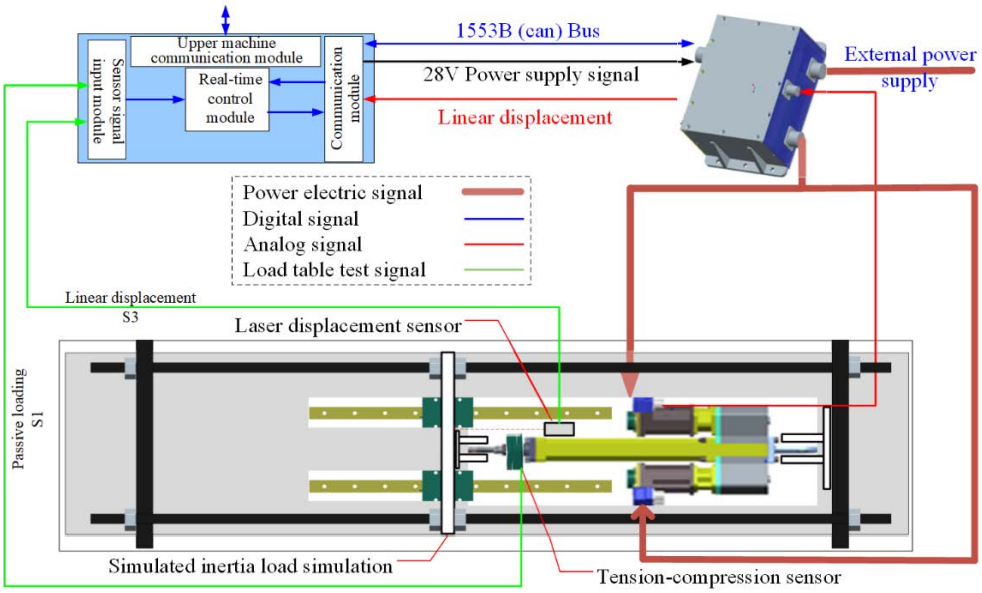


**FIGURE 7.** Working principle of the load simulation platform of the actuation system.

and the stiffness of the elastic load is eight times that of the single spring.

The inertial load simulation unit mainly simulates the inertial load of the rudder, which consists of a sliding plate and its attachments. Based on conservation of kinetic energy, the mass of the slider is designed to be

$$m_{ac} = J_{pl}\left[\frac{\Delta\theta_{pl}\pi/180^{\circ}}{L_{AB} - \sqrt{L_{OA}^2 + R^2 - 2L_{OA}Rcos\left(\theta_0 - \Delta\theta_{pl}\right)}}\right]^2 \tag{14}$$

### B. CONTROL AND TEST SYSTEM DESIGN OF THE LOAD SIMULATION PLATFORM

The control and test system of the load simulation platform mainly includes a real-time control module, data acquisition module, servo motor driver, displacement sensor, and tension-compression sensor. Fig. 7 demonstrates the working principle of the control and test system. The displacement sensor is located inside the actuator for the real-time monitoring of the actuator position for closed-loop control; the tension-compression sensor is connected in series between the EMA and the elastic simulated load, and its real-time data are displayed on the oscilloscope, which can visually demonstrate the impact of the actuator on the simulated load.

In this system, the real-time control module achieves the offline drive of the differential actuator, which is the core element of the load simulation platform, and is responsible for receiving the motion control signals from the upper machine, and comparing them with the collected displacement sensor signals and the EMA position data. After the control method and strategy are selected, the control unit of the servo motor driver converts the command signal into three-phase voltage and current signals to drive the servo motor of the EMA, which drives the analog load. Meanwhile, the signal of the tension-compression sensor and the actuator position data are sent back to the data acquisition system.

During the break-in experiment on the brake, the operating state of a channel needs to be changed, and the real-time control module needs to send an ON/OFF command to the corresponding electromagnetic brake in accordance with the command of the break-in and lock working mode. Under the ON state, the brake is de-energized and inactive; under the OFF state, the electromagnetic brake is energized and the armature attracts the yoke to lock the channel.

## IV. EXPERIMENTAL DESIGN AND RESULTS ANALYSIS OF SYSTEM BREAK-IN PROCESS

Considering a certain type of differential actuator as the research target, through the above analysis, we designed an on-machine break-in experiment, and the related experimental results were analyzed.

### A. EXPERIMENTAL DESIGN

The specific simulation scenarios for the simulated loads under different constrained states on the test bench are as follows.

(1) Free-state simulation of the load: The output end of the top rod of the actuator was connected to the connection socket of the load platform, which was mounted on the linear guide slider and could simulate the free state of the load, i.e., the pull rod of the actuator could extend and retract freely.

(2) Fixed-state simulation of the load: The connecting socket was fixed with the test bench frame via tooling, and could be used to simulate the state where the load position was fixed, i.e., the pull rod of the actuator was not retractable.

The designed and assembled load simulation platform is shown in Fig. 8.

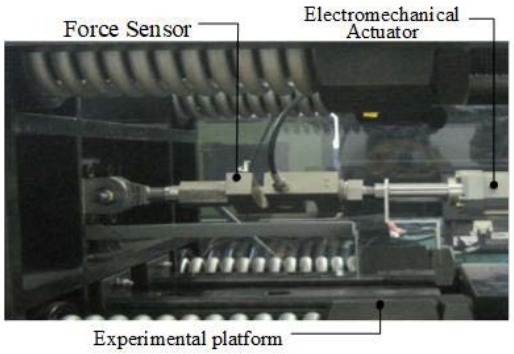


**FIGURE 8.** Components of the load simulation platform.

The magnitude of the impact forces generated by the brake unit on the load was simulated during the break-in start and stop processes under the two boundary conditions, i.e., fixed or free. The relevant experimental conditions for the break-in experiment are shown in Table 2.

**TABLE 2.** Conditions of the experiment.

| Project | | Unit | Value |
|---|---|---|---|
| Motor Speed | | Rpm | ±400 |
| Travel Limit | | Mm | -20–20 |
| Total Break-in Time | | S | 240 |
| Brake Start Stop Command | Single Unlocking Time | S | 0.1 |
| | Single Lock Time | S | 0.1 |

According to the break-in and lock proposal from the brake unit manufacturer, the break-in and lock time sequence in this experiment is shown in Fig.9. When the order value was 1, the electromagnetic brake was de-energized and the channel was in an unlocked state; when the order value was 0, the electromagnetic brake was energized and the channel was in a locked state. The brake started to break-in by means of a break-in start/stop command, and the impact on the load under different break-in conditions was obtained by the pull pressure sensor placed on the top rod of the actuator.

The detailed procedures for the break-in experiment are as follows.

(1) Installing the test sample and force transducer.

(2) Adjusting the slider mounting status according to the set break-in working mode.

(3) The actuator system starting and controlling the corresponding transmission channels according to the defined working modes, the closed-loop controlling of the speed loop, and the load simulator remaining in a free or fixed state according to the defined working mode.

(4) Initiating the break-in and lock start/stop control and executing the break-in and lock procedure.

(5) Recording the reading $F_a$ of the force transducer.

According to engineering experience, the magnitude of the impact of the actuator on the load in this servo system is in the range of 0.5–6 kN. In this experiment, the force transducer was selected with a sensitivity of 100 mV/kN.

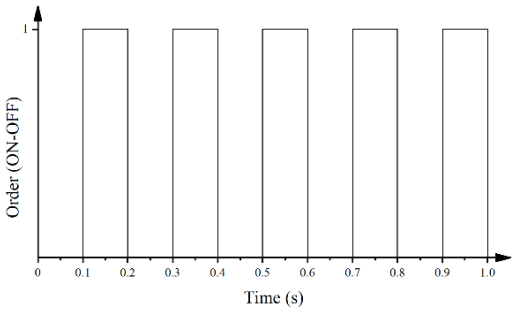


**FIGURE 9.** Time sequence of the brake start/stop command.

### B. RESULTS AND ANALYSIS

Based on the result analysis of the three break-in and lock working modes in the experiment, it can be observed that

(1) Under Mode 1, the system was in a single-degree-of-freedom state with a single input and a single output. The force transducer readings are shown in Fig. 10, which indicated that the maximum impact generated was approximately 3 kN, with some blurs peaking up to 3.5 kN.

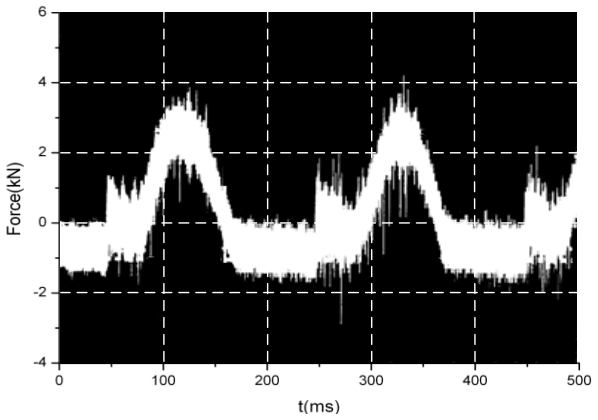


**FIGURE 10.** Axial force of the actuator under Mode 1.

From 0–100 ms, the system was in the break-in and lock phase, and the load was in the upward phase and reached the maximum value; from 100–200 ms, the system was in the unlocking phase and the load was in the downward phase until it reached 0; throughout the break-in and lock cycle, the load appeared to be half-sine.

As the motor is an AC permanent magnet synchronous servo motor, under this working mode, the Channel A motor drives the Channel B motor to rotate, and the output motor works in the electronic generator state. There is a charging and discharging process between the electronic generator and the capacitance on the DC bus, so a half sine wave will appear, and the rising part of the half sine wave is the process of charging the capacitance on the bus by the electricity from the generator, and the falling part is the process of discharging the

voltage on the capacitance through the motor after the motor stops rotating.

(2) Under Mode 2, the system was in a single-degree-of-freedom state with a single input and a single output. The force transducer readings are shown in Fig. 11, which indicated that the maximum impact generated was approximately 3 kN, with a small amount of blurs peaking up to 4 kN.

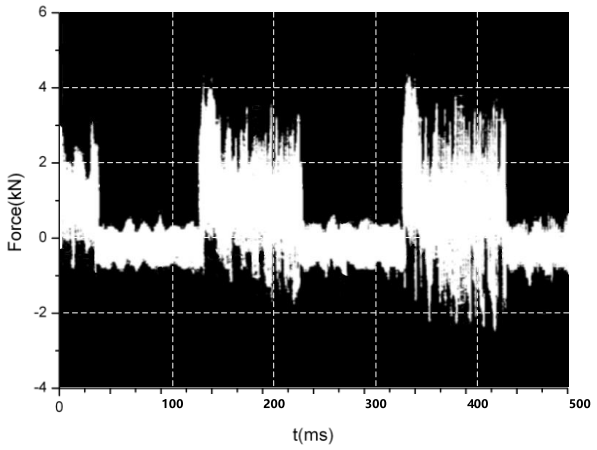


**FIGURE 11.** Axial force of the actuator under Mode 2.

Under this working mode, the Channel A motor needed to drive the simulated load, and the output is in pure mechanical mode. Because the Channel A motor is in speed loop control, not torque loop control, the force measurement value will present a certain degree of fluctuations. In addition, a large starting torque is required in the initial stage, which will bring relatively large impact force. Owing to the uniqueness of the freedom of movement, the system had a high rotational speed, which increased the viscous friction of the system and generated the largest impact among the three modes in the unlocking phase.

(3) Under Mode 3, the system was in a multiple-degrees-of-freedom state with a single input and multiple outputs. The force transducer readings are shown in Fig. 12, which indicated that the maximum impact generated was approximately 2 kN, with a small amount of blurs peaking up to 3 kN.

The results show that the load fluctuated up and down around 2 kN during the broken-in and locked phase, and around −1 kN during the unlocking phase. Under this mode, there were two parallel channels in the motion loop and two outputs. During the break-in process, both outputs were in motion and operated at a lower speed than those under the other two modes. Thus, the viscous friction of the system was relatively low, generating the smallest impact.

From the above tests, it is concluded that

(1) Under Mode 3, when the rudder surface is in a free state, one channel is in a broken-in and locked state, and the other channel is in an unlocked state, the break-in and lock has the smallest impact on the rudder surface, as shown in Fig. 13.

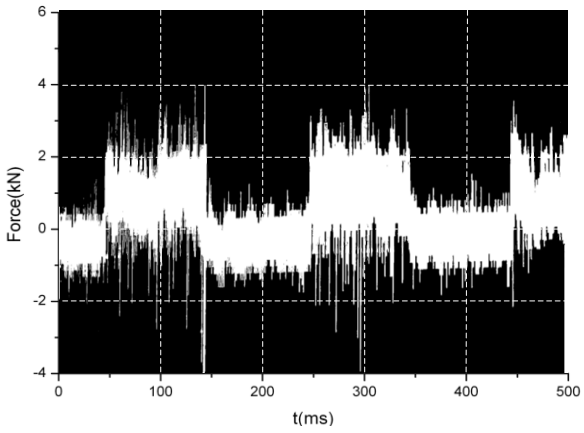


**FIGURE 12.** Axial force of the actuator under Mode 3.

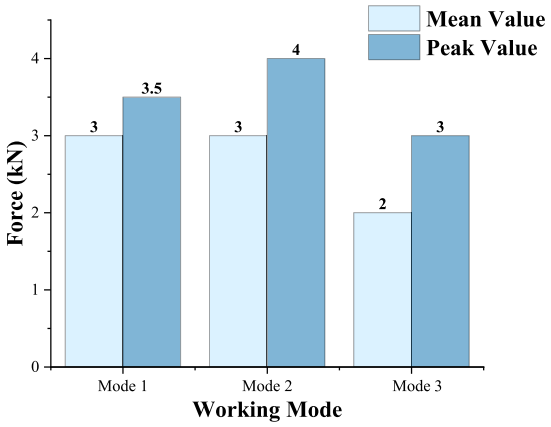


**FIGURE 13.** Impact of actuator on the load under each working mode.

(2) When the rudder surface is in a free state, one channel is in a broken-in and locked state, and the other channel is in an unlocked state, the actuation rod will retract and the unlocked channel will also generate motion, which is related to the fact that the impact generated by the broken-in and locked channel is slightly larger than the frictional resistance between the actuation rod and the unlocked channel.

(3) The drastic increase in load at the initial moments of the unlocking phase under all three working modes is due to the fact that Modes 2 and 3 exhibit a large starting torque because of the greater load inertia and greater acceleration torque requirements compared with those in Mode 1.

## V. CONCLUSION

In this study, we first analyzed the dynamics of the three working modes of a differential redundant actuation system. Accordingly, we proposed three feasible break-in working modes of the brake unit. Subsequently, we designed a load simulation platform of the actuation system, through which the offline simulation operation of various load characteristics of the actuation system was achieved. Using this platform, we designed an offline experimental protocol for the

impact of the differential redundant actuation system on the load during the break-in process, and analyzed the impact of the brake unit on the load under the conditions of different break-in working modes through the experiment. We also analyzed the variation pattern of the impact. The experimental results show that, when the differential redundant actuation system is in a multiple-degrees-of-freedom state with a single input and multiple outputs, the impact on the load during the break-in process of the brake unit is the smallest, and when the load of the differential redundant actuation system is in a locked state, the impact on the load during the break-in process of the brake unit is the largest.

## NOMENCLATURE

| | |
|---|---|
| $J_i$ | Rotational inertia of gear i (i = 1,2, 3, 4, 5,6). |
| $J_{2g}$ | Moment of inertia of planetary gear 2. |
| $J_{2z}$ | Rotational inertia of planetary gear 2. |
| $J_H$ | Rotational inertia of the planetary carrier. |
| $J_{pl}$ | Rotational inertia of rudder. |
| $r_i$ | Radius of gear i (i = 1,2, 3, 4, 5,6). |
| $r_{2g}$ | Radius of revolution of the planetary gear. |
| $r_{2z}$ | Radius of the planetary gear. |
| $r_H$ | Distance between the center of the planetary gear and the center of the planetary carrier. |
| $\varepsilon_i$ | Angular acceleration of gear i (i = 1,2, 3, 4, 5,6). |
| $\varepsilon_{2g}$ | Angular acceleration of the revolution of the planetary gear. |
| $\varepsilon_{2z}$ | Angular acceleration of the rotation of the planetary gear. |
| $\varepsilon_H$ | Angular acceleration of the planetary carrier. |
| $m_2$ | Mass of the planetary gear. |
| $m_{ac}$ | Slider mass of the inertial load simulation unit. |
| $f_{1o}$ | Frictional resistance of Channel B. |
| $f_H$ | Frictional resistance of the output channel of the planetary carrier. |
| $F_i$ | Tangential drive of gear i (i = 1,2, 3, 4, 5,6). |
| $F_{Sl}$ | Loading force of a single spring on the left side of the load simulation platform. |
| $F_{Sr}$ | Loading force of a single spring on the right side of the load simulation platform. |
| $F_{Lk}$ | Total elastic loading force. |
| $T_{imA}$ | Torque of input A under working mode i (i = 1, 2, 3). |
| $T_{mB0}$ | No-load torque of Channel B motor. |
| $T_{fAB}$ | Frictional torque between Channels A and B. |
| $T_{fAL}$ | Frictional resistance torque between Channel A and load. |
| $T_{fAH}$ | Frictional resistance torque from the input of Channel A to the output of the planetary carrier. |
| $T_{fac}$ | Frictional resistance torque of the actuator assembly. |
| $T_{fL}$ | Frictional resistance torque of the load. |
| $T_{fH}$ | Frictional resistance torque of the output channel of the planetary carrier. |
| $T_{f1o}$ | Frictional resistance torque of Channel B. |
| $L_{AB}$ | Initial length of actuator. |
| $L_{OA}$ | The distance from the rudder shaft to the fixed hinge end of the actuator. |
| $L_0$ | Initial preload displacement of the spring. |
| $x$ | Working stroke of the actuator under test. |
| $R$ | Length of rocker arm in the Rudder Loop. |
| $\theta_0$ | Initial rudder deflection angle. |
| $\Delta\theta_{pl}$ | Variation of the rudder deflection angle. |

## REFERENCES

[1] S. Ijaz, M. T. Hamayun, L. Yan, H. Ijaz, and C. Shi, "Adaptive fault tolerant control of dissimilar redundant actuation system of civil aircraft based on integral sliding mode control strategy," *Trans. Inst. Meas. Control*, vol. 41, no. 13, pp. 3756–3768, Sep. 2019.
[2] S. Ljaz, L. Yan, M. T. Hamayun, and C. Shi, "Active fault tolerant control scheme for aircraft with dissimilar redundant actuation system subject to hydraulic failure," *J. Franklin Inst.*, vol. 356, no. 3, pp. 1302–1332, Feb. 2019.
[3] L. Tian, Y. S. Zhang, and H. W. Wang, "Research on modeling and force dispute equilibrium of fly by wire flight control actuation system," *J. Northwest Univ. Technol.*, vol. 38, no. 3, pp. 643–648, 2020.
[4] D. X. Huang, "Research on mode switching control strategy and switching quality evaluation of car electromagnetic and friction integrated braking system," Ph.D. dissertation, Dept. Vehicle Eng. College, Jiangsu Univ., Zhenjiang, China, 2020.
[5] G. R. Cai, "Research on friction and wear performance and structural optimization design of disc brake lining," M.S. thesis, Dept. Vehicle Eng. College, Jiangsu Univ., Zhenjiang, China, 2019.
[6] H. S. Xu, "Tribology technology and properties of micro texture on friction pairs of rolling bearings," M.S. thesis, Dept. Vehicle Eng. College, Jiangsu Univ., Zhenjiang, China, 2018.
[7] G. D. Sun, "Research on characterization and prediction modeling of running in attractor," M.S. thesis, Dept. Mech. Eng. College, Mining Technol. Univ., Xuzhou, China, 2019.
[8] G. P. Zhang, "Research on theory and method of sliding wear prediction based on surface morphology," Ph.D. dissertation, Dept. Mech. Eng. College, Huazhong Sci. Technol. Univ., Wuhan, China, 2013.
[9] Y. S. Zhang, X. M. Kong, and D. R. Chen, "Computer simulation of the change of surface morphology of cylinder liner in running in process," *J. Tribology*, vol. 19, no. 2, pp. 56–60, 1999.
[10] M. Mohammad, A. Mohammad, and T. Shahrzad, "Autonomous shock sensing using bi-stable triboelectric generators and MEMS electrostatic levitation actuators," *Smart Mater. Struct.*, vol. 30, no. 6, pp. 13–26, 2021.
[11] C. Y. Fu and L. H. Cao, "Impact strength analysis of fire and explosion emergency exit door actuator," *J. Prog. Aviation Eng.*, vol. 9, no. 1, pp. 107–110, 2018.
[12] D. Li, B. Li Bin, and X. M. Liu, "Aerodynamic load analysis of folding rudder deployment process of air-to-air missile," *J. Missile Guid.*, vol. 34, no. 3, pp. 154–156, 2014.
[13] S. Wang, "Research on load torque simulation technology of steering gear of high-speed aircraft," Ph.D. dissertation, Dept. Control Simul. Eng. College, Harbin Eng. Univ., Harbin, China, 2013.
[14] W. Zhang, "Research on dual motor cooperative control system based on servo actuator," M.S. thesis, Dept. Mech. Eng. College, Dongnan Univ., Nanjing, China, 2019.
[15] T. Liu, G. P. Zhao, H. Y. Yan, and P. J. Cui, "Differential fault switching and mode analysis under friction load," *J. Mech. Transmiss.*, vol. 42, no. 12, pp. 123–128, 2018.
[16] B. Gao, Y. L. Fu, Z. C. Pei, and J. M. Ma, "Research on dual-variable integrated electro-hydrostatic actuator," *Chin. J. Aeronaut*, vol. 19, pp. 77–82, Dec. 2006.

**PEIJUAN CUI** was born in Jiangsu, China, in 1983. She received the B.S. and M.S. degrees in mechanical engineering from the University of Science and Technology Beijing, China, in 2006 and 2009, respectively. She is currently pursuing the Ph.D. degree in electrical engineering with the Harbin Institute of Technology. Her current research interests include multi-objective optimization design of electro-mechanical servo systems and control methods applied to fault-tolerant systems.

**QIANFAN ZHANG** (Member, IEEE) was born in Heilongjiang, China. He received the B.S. and Ph.D. degrees in electrical engineering from the Harbin Institute of Technology, Harbin, China, in 1999 and 2004, respectively. In 1999, he joined the Department of Electrical Engineering, Harbin Institute of Technology, as a Faculty. He has been a Professor, since 2010. His research interests include electric vehicle, hybrid electric vehicle, and photovoltaic applications.

**ZHANLIN HOU** was born in Hebei, China, in 1985. He received the B.S. degree in mechanical engineering and automation from the Beijing University of Aeronautics and Astronautics, in 2015. He is currently a Designer with the Beijing Institute of Precision Mechatronics and Controls. His research interests include design and testing of electromechanical actuators and their constituent components.

**YUPING HUANG** was born in 1967. He received the B.Sc. degree in automatic control from Shanghai Jiao Tong University, Shanghai, China, in 1989, and the M.Sc. degree in hydraulic transmission and control from the China Academy of Launch Vehicle Technology, Beijing, China, in 1992. He is currently a Professor and the Ph.D. Candidate Supervisor with the Beijing Institute of Precision Mechatronics and Controls, China. His research interests include dynamics and control of aerospace servo systems, complicated mechatronics systems, and robots.

**LUMAN HE** was born in Fujian, China, in 1997. She received the B.S. degree in smart grid information engineering from the Nanjing University of Posts and Telecommunications, Nanjing, China, in 2020. She is currently pursuing the M.S. degree in mechanical engineering with the Beijing Institute of Precision Mechatronics and Controls. Her research interests include control methods of redundancy and fault-tolerant systems.

**ZAIPING ZHENG** was born in Zhejiang, China, in 1979. He received the B.Sc. degree in automation from Harbin Engineering University, Harbin, China, in 2002, and the M.Sc. degree in control engineering from the Beijing University of Aeronautics and Astronautics, Beijing, China, in 2012. He is currently pursuing the Ph.D. degree in electrical engineering with the Harbin Institute of Technology. His current research interests include control methods applied to multiphase fault tolerant permanent magnet synchronous machines and PMSM systems.